Combustion and Flame 223 (2021) 181–191

Contents lists available at ScienceDirect

Combustion and Flame

journal homepage: www.elsevier.com/locate/combustflame

Role of low-temperature oxidation in non-uniform end-gas autoignition and strong pressure wave generation

Hiroshi Terashima[a,*], Hisashi Nakamura[b], Akira Matsugi[c], Mitsuo Koshi[d]

[a] Division of Mechanical and Aerospace Engineering, Hokkaido University, N13 W8, Kita-ku, Sapporo, Hokkaido 060–8628, Japan
[b] Institute of Fluid Science, Tohoku University, 2-1-1 Katahira, Aoba-ku, Sendai, Miyagi 980–8577, Japan
[c] National Institute of Advanced Industrial Science and Technology, 16-1 Onogawa, Tsukuba, Ibaraki 305–8569, Japan
[d] The University of Tokyo, 7-3-1 Hongo, Bunkyo-ku, Tokyo 113–8654, Japan

ARTICLE INFO

Article history:
Received 17 May 2020
Revised 21 September 2020
Accepted 21 September 2020
Available online 14 October 2020

Keywords:
Low-temperature chemistry
End-gas autoignition
Knocking combustion
Detailed chemistry

ABSTRACT

This study highlights the importance of heat release rate in low-temperature oxidation (LTO) on non-uniform end-gas autoignition and strong pressure wave generation, which are substantially relevant to knocking combustion. The simulations are conducted using the compressible Navier–Stokes equations with detailed transport and chemical kinetics models in a one-dimensional constant-volume reactor. Four fuel/air stoichiometric mixtures, *n*-butane, *i*-octane, *n*-heptane, and dimethyl ether (DME)/air mixtures, are simulated. The results show that larger knocking intensities are produced with *n*-heptane and DME in their negative temperature coefficient (NTC) regimes because of the stronger non-uniformity of end-gas autoignition. The non-uniformity of end-gas autoignition is enhanced by a pressure wave disturbance that is caused by the rapid temperature rise of the end-gas region in LTO. In particular, the high heat release rate with the DME/air mixture generates a distinct pressure wave disturbance in the reactor, which considerably enhances the non-uniformity of end-gas autoignition through the reflection of the wave at the wall. In contrast, the heat release rate in the *n*-heptane case is milder than that in the DME case, and therefore, the knocking intensity in the *n*-heptane case is smaller compared to that of DME due to less enhancement of the non-uniform end-gas autoignition. No large knocking intensities are produced with *n*-butane and *i*-octane, which have weak NTC, because of the absence of a temperature rise in LTO. Thus, this study concludes that the high heat release rate in LTO and the generated pressure wave disturbance play a significant role in the generation of large knocking intensities through the enhancement of non-uniform end-gas autoignition.

1. Introduction

Knocking combustion is a well-known abnormal combustion that happens in spark-assisted ignition engines [1]. Knocking is generally initiated by autoignition in the region between a propagating flame and an engine wall. Such autoignition and region are commonly called end-gas autoignition and the end-gas region, respectively. A pressure wave is then generated through rapid heat release in the end-gas region, which is sometimes strengthened by a coupling with a reaction front wave [2,3]. Such a strong pressure wave may cause severe engine damage during the subsequent pressure oscillation. Undoubtedly, knocking combustion is still a significant obstacle in achieving the desired high thermal efficiency in advanced internal combustion engines [4].

Because knocking combustion is a consequence of the competition between the propagating flame speed in an engine cylinder and timing of end-gas autoignition, the ignition delay time of an employed fuel is one of the most influential parameters in knocking combustion. The ignition delay time generally changes according to the thermodynamic conditions, such as pressure, temperature, and fuel concentration, of which the negative temperature coefficient (NTC) may be highlighted as a unique characteristic observed in large hydrocarbon fuels, including gasoline fuels [5]. In an NTC regime, the ignition delay time becomes longer despite the temperature increase, which affects the timing of end-gas autoignition. The negative temperature dependence of ignition delay time is a consequence of the two-stage ignition in the temporal temperature variation, which consists of a first temperature rise caused by low-temperature chemistry and a second temperature rise governed by high-temperature chemistry [5].

It is natural to seek for the effects of the NTC and low-temperature chemistry on knocking combustion owing to the

* Corresponding author.
E-mail address: htera@eng.hokudai.ac.jp (H. Terashima).

https://doi.org/10.1016/j.combustflame.2020.09.025
0010-2180/

above-mentioned unique behaviors. Many studies have been conducted to identify the effect of an NTC on knocking combustion. In particular, the effect of an NTC on strong pressure wave generation triggered by hot- or cool-spot autoignition has been extensively investigated [6–11] following the pioneering works by Zel'dovich [2] and Bradley's group [3,12]. For example, Dai et al. [6] demonstrated that a pressure wave generated by cool-spot autoignition became a developing detonation wave owing to the NTC characteristic of an *n*-heptane/air mixture. Zhang et al. [11] investigated the effects of low-temperature chemistry on pressure wave formation under thermal and fuel stratifications of dimethyl ether (DME)/air mixtures, where a unique comparison was conducted using an original reaction mechanism and a modified reaction mechanism created by removing some critical reactions of the low-temperature chemistry. The study showed that the low-temperature chemistry had a significant effect on the ignition-to-detonation transition through a difference in the ignition delay time caused by the different reaction mechanisms with and without low-temperature chemistry. Those previous studies demonstrated that the effect of an NTC on pressure wave development emerges from the spatial gradient in the ignition delay time established by thermal or fuel stratifications. The NTC behavior of employed fuel/air mixtures affects the spatial gradient or distribution of the ignition delay time, which determines the successive autoignition phenomena (i.e., the speed of a reaction front wave) and, thus, the pressure wave development. Experimentally, strong pressure waves are often observed with NTC fuels. Tanoue et al. [13] showed that stronger pressure waves were generated as the fraction of DME in *n*-butane/DME/air mixtures increased in a rapid compression machine (RCM) experiment. The mechanism for strong pressure wave generation was well explained by assuming the presence of a spatial gradient in the ignition delay time due to temperature stratifications. Mansfield et al. [14] addressed non-uniform and uniform autoignition behaviors of *i*-octane in two RCMs, assuming the existence of temperature gradients. Interestingly, it was suggested that the propensity for uniform autoignition increased in the NTC regime because the temperature sensitivity of the ignition delay time decreased. Pan et al. [15] quantified the combustion modes of strong knocking in an RCM experiment using a non-dimensional regime diagram with estimated temperature stratifications. From a different viewpoint, Pan et al. [16] numerically investigated the behaviors of end-gas autoignition and pressure wave development of an *n*-heptane/air mixture under the assumption that a two-stage flame was present through cool flame generation. The result showed that the autoignition and subsequent pressure wave formation with the two-stage flame were different from those using an ordinary single-stage flame. Thus, the NTC characteristic has the potential to significantly affect the important process of knocking combustion.

This study aims to identify further the effect of fuel NTC characteristics on end-gas autoignition and subsequent pressure wave formation. Particular attention is paid to the role of two-stage ignition, that is, small temperature rise in a temporal variation caused by low-temperature chemistry, which has not been addressed in previous studies. This study started from our previous study [17], which showed that an *n*-heptane/air mixture with an NTC behavior generated a strong pressure wave only in the NTC regime. Unfortunately, the reason has not yet been fully explained in the subsequent studies [18,19]. A one-dimensional (1-D) constant-volume configuration is used for the investigation, where the compressible Navier-Stokes equations are solved with detailed transport and chemical reaction models, and four different fuel/air stoichiometric mixtures are adapted.

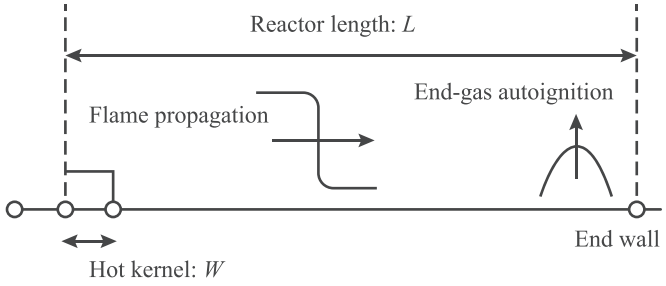

Fig. 1. Schematic of a one-dimensional constant-volume reactor.

2. Numerical methods

The governing equations are the compressible Navier–Stokes equations with the thermally perfect gas equation of state. The CHEMKIN-II library [20] was used to calculate the thermodynamic properties. The transport properties for mixtures were obtained using a software package [21], where the viscous coefficient of mixtures is modeled by an empirical approximation [22] that is analogous to the thermal conductivity [21]. The species bundling technique [23] was applied to the mixture-averaged diffusion coefficient to significantly reduce the computational cost. An operator splitting method [24] was applied to the governing equations; that is, the fluid and chemical reaction parts were solved separately in the temporal direction. In the fluid part, the compressible Navier–Stokes equations were solved by assuming chemically frozen flows of $\dot{\omega}_s = 0$. In the chemical reaction part, the governing equations derived from the compressible Navier–Stokes equations under constant volume and internal energy conditions were solved. Variables were exchanged between the fluid and chemical reaction parts at each time step [25].

Conventional numerical methods for the compressible Navier–Stokes equations were used in the fluid part. The numerical flux was evaluated by using a Harten–Lax-van Leer-contact scheme [26]. The monotone upstream centered scheme for conservation law [27] with the minmod limiter was used to achieve high-order spatial accuracy. The viscous, heat conductivity, and diffusion terms were discretized by second-order central differencing. The third-order total variation diminishing Runge–Kutta scheme [28] was applied to the time integration. In the chemical reaction part, the extended robustness-enhanced numerical algorithm [29], called ERENA, was applied to the time integration for the chemical reaction equations. More detailed description on the numerical models and methods can be found in our previous articles [17,18].

3. Conditions

A 1-D constant-volume reactor was used for this investigation, which has been successfully applied in several numerical studies [17,30–32] to investigate the fundamental physics relevant to knocking combustion, such as end-gas autoignition and the subsequent pressure wave development. A schematic of the 1-D reactor is shown in Fig. 1. A flame generated by the ignition of a hot kernel propagates rightward, and an end-gas region is established between the propagating flame and the end wall. As the pressure and temperature in the reactor gradually increase owing to the flame propagation, end-gas autoignition may eventually occur, followed by strong pressure wave generation. The reactor length was $L = 4$ cm, and a 1400 K hot kernel was used with a size of $W = 0.1$ cm, unless otherwise noted. The ignition of the hot-temperature kernel induces not only the flame propagation but also a pulsed pressure wave. It should be noted that the strength of the pulsed pressure

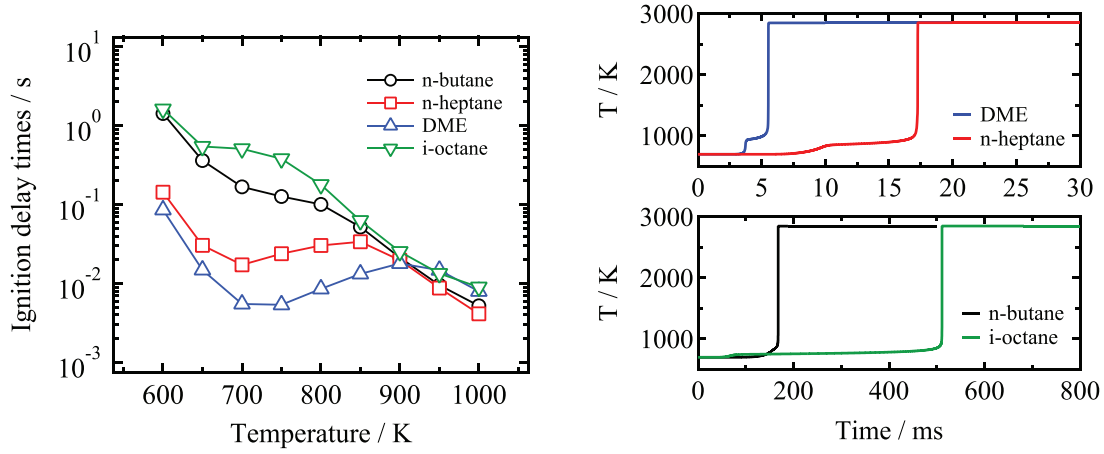

Fig. 2. Ignition delay times for four fuel/air stoichiometric mixtures under 5 atm (left), and time histories of temperature at 700 K (right).

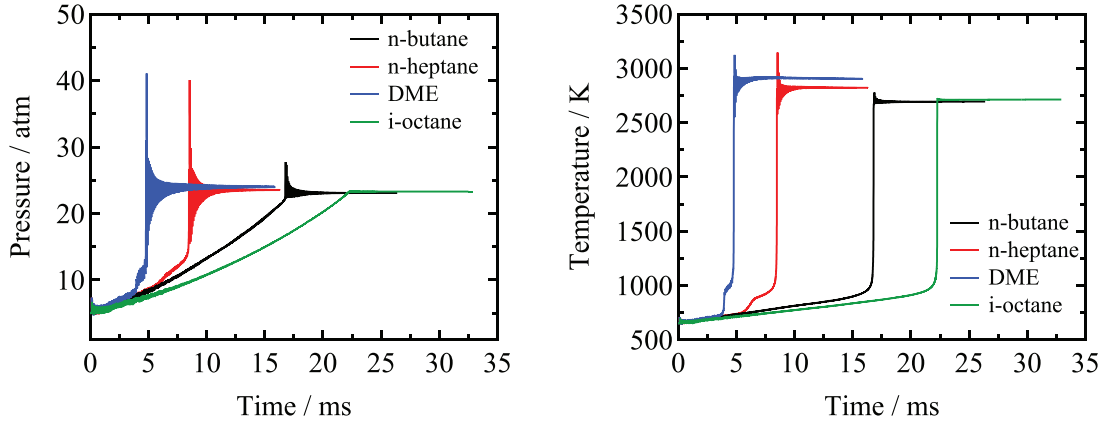

(a) Initial temperature, 650 K

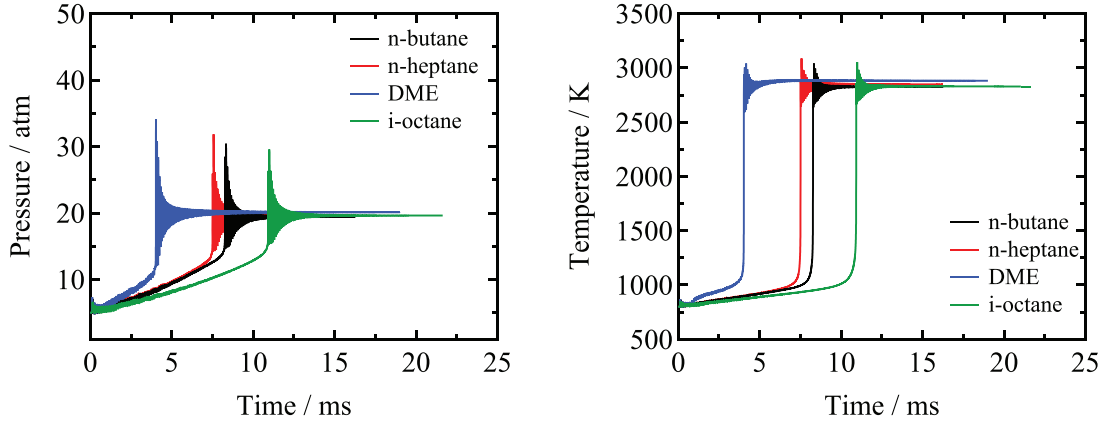

(b) Initial temperature, 800 K

Fig. 3. Comparison of time histories of the pressure (left) and temperature (right) at the wall for different initial temperatures.

wave may be strong due to the present 1-D planar configuration compared to one generated in actual engines. The effects of the hot-kernel size on end-gas autoignition and subsequent pressure wave development were discussed in our previous study [19]. A symmetric condition was applied at the left boundary, and an adiabatic wall was assumed at the right boundary. The effects of the end-wall conditions (adiabatic and isothermal) were also discussed in our previous studies [17–19]. The initial pressure was set to 5 atm and the initial temperature changed from 500 K to 1000 K.

Four fuels were used at stoichiometric conditions with air: *n*-heptane, DME, *n*-butane, and *i*-octane. The detailed chemical reaction mechanisms for *n*-heptane, *n*-butane, and *i*-octane were generated by the KUCRS software [33], where *n*-heptane consisted of 373 species with 1071 reactions, *n*-butane consisted of 113 species with 426 reactions, and *i*-octane consisted of 537 species with 1470 reactions. The prediction accuracy of the mechanisms generated by KUCRS was validated through a comparison with experimental data in our previous study [17] for *n*-heptane and *n*-butane,

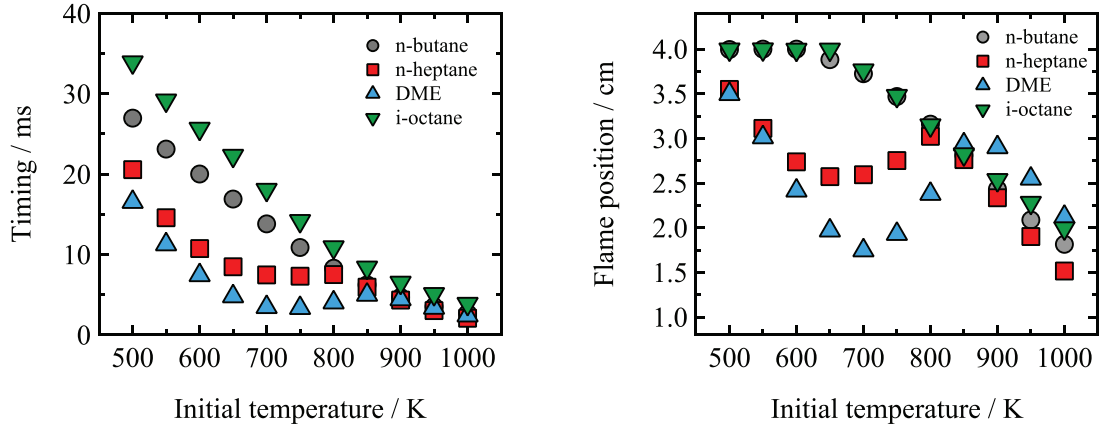

(a) Timing (b) Flame position

Fig. 4. Timing and flame position when end-gas autoignition takes place. The timing corresponds to the time when the first peak in the maximum pressure history is observed and the flame position was determined as the position when a flame front reaches the maximum distance from the left boundary.

and a study [34] for *i*-octane. The mechanism proposed by Zhao et al. [35] was used for DME, which consisted of 55 species involving 290 reactions. Figure 2 shows the ignition delay times at various temperatures obtained using four fuel/air stoichiometric mixtures under 5 atm, and constant volume and adiabatic conditions. An NTC in the ignition delay time is observed between 700 K and 850 K for the *n*-heptane and DME/air mixtures. The NTC is connected to a two-ignition process, in which a small temperature rise due to low-temperature oxidation (LTO) appears before the main autoignition, as observed in the right-hand side of Fig. 2. In the following discussion, we may use the term 'strong NTC fuel' for *n*-heptane and DME and the term 'weak NTC fuel' for *n*-butane and *i*-octane, respectively, for convenience.

A uniform grid spacing of approximately 20 μm was used based on a preliminary grid convergence study [17]. The time step size was determined with a CFL number of 0.8. In the species bundling technique [23] used for the diffusion coefficient calculation, DME with 55 species was bundled into 17 groups, *n*-butane with 113 species into 19 groups, *n*-heptane with 373 species into 21 groups, and *i*-octane with 537 species into 23 groups, with a threshold value of 0.1.

4. Results and discussions

In the following discussions, a knocking intensity is introduced to quantitatively estimate the behavior of a pressure wave initiated by end-gas autoignition, which is defined as the ratio of the first peak in the maximum pressure history in the entire domain to the equilibrium pressure [17]. Thus, the knocking intensity here is a metric to assess the strength of a pressure wave developed in the end-gas region.

4.1. Comparison with four fuels

Figure 3 (a) shows a comparison of the pressure and temperature histories at the wall with an initial temperature of 650 K using the four fuels. Significant pressure peaks associated with the occurrence of end-gas autoignition are observed for *n*-heptane and DME. In contrast, no pressure peaks are generated by *i*-octane, which means that the propagating flame from the hot kernel reaches the end wall before end-gas autoignition can occur. A small pressure peak for *n*-butane indicates that autoignition takes place with a small amount of the end gas, and thus a pressure wave cannot develop. In the *n*-heptane and DME cases, a relatively small temperature rise appears before the main autoignition owing to LTO. Further, especially in the DME case, a distinct pressure oscillation

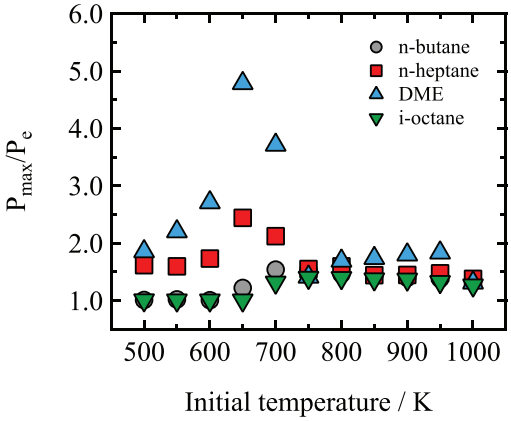

Fig. 5. Knocking intensities against the initial temperature.

appears along with the small temperature rise by LTO. Such a temperature rise associated with LTO is not observed with *n*-butane and *i*-octane. The result for the higher initial temperature of 800 K in Fig. 3(b) depicts that end-gas autoignition occurs with all the fuels due to the high-temperature condition and thus the shorter ignition delay times. The small temperature rise by LTO becomes weak or almost disappears at 800 K.

Figure 4 summarizes the timing and the flame position when end-gas autoignition occurs. The timing results demonstrate a close relationship between the timing and the fuel characteristics of the ignition delay time (shown in Fig. 2): the shorter the ignition delay time, the faster end-gas autoignition occurs. In the NTC regimes, the flame position is significantly affected by the fuel characteristics, and broader end-gas regions remain for strong NTC fuels: *n*-heptane and DME. It is also confirmed that no end-gas autoignition occurs for temperatures below 600 K in *n*-butane and 650 K in *i*-octane, respectively. Figure 5 shows the knocking intensity against the initial temperature. A substantial peak is generated around 650 K in the DME case, and a relatively smaller, yet still large, peak is also observed in the *n*-heptane case. These peaks imply that strong pressure waves are generated, so-called developing detonation waves. In contrast, no peaks are produced in the cases of *n*-butane and *i*-octane, and thus the knocking intensity remains small for all the initial temperatures. The trend of the knocking intensities suggests that strong NTC fuels (*n*-heptane and DME) may have the potential to produce large knocking intensities in their NTC regimes through the generation of strong pressure waves.

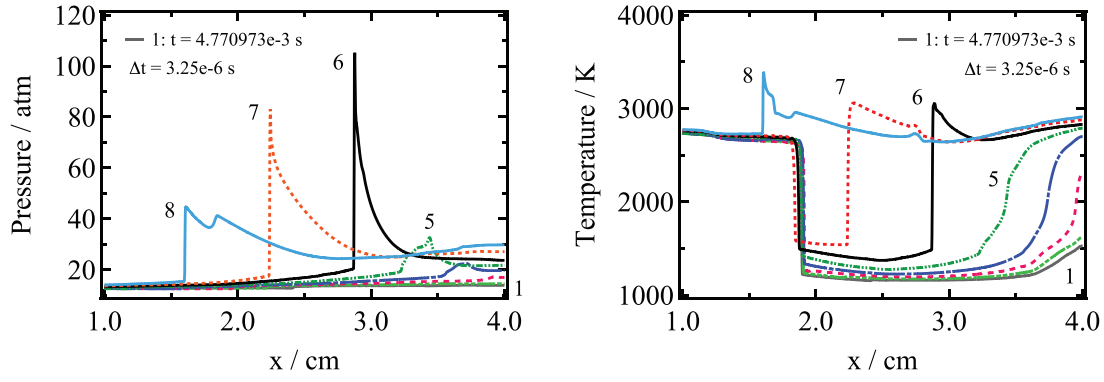

(a) DME

(b) *n*-heptane reproduced from [17]

Fig. 6. Temporal sequence of pressure and temperature distributions for an initial temperature of 650 K.

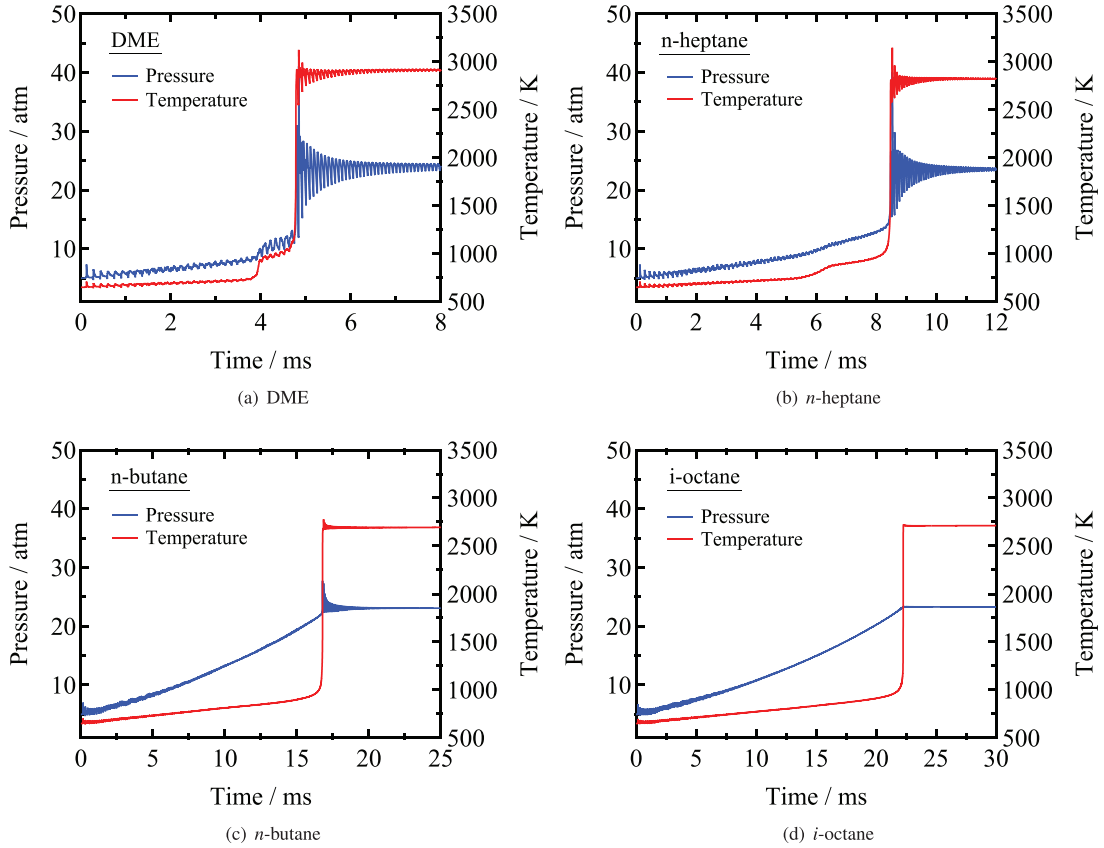

(a) DME

(b) *n*-heptane

(c) *n*-butane

(d) *i*-octane

Fig. 7. Time histories of the pressure and temperature at the wall for each fuel with an initial temperature of 650 K.

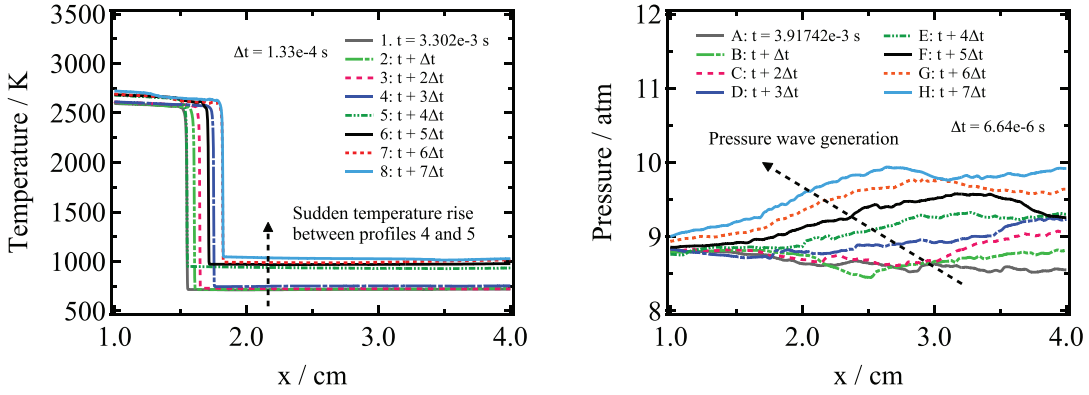

(a) Sudden temperature rise (b) Pressure wave generation due to sudden temperature rise

Fig. 8. Behaviors of temperature and pressure during LTO at 650 K for the DME case. Note that the time period (Δt) differs in two-order between the left and right figures. The right figure (b) shows the pressure wave behavior during the period between the profiles 4 and 5 in the temporal sequence of temperature in the left figure (a).

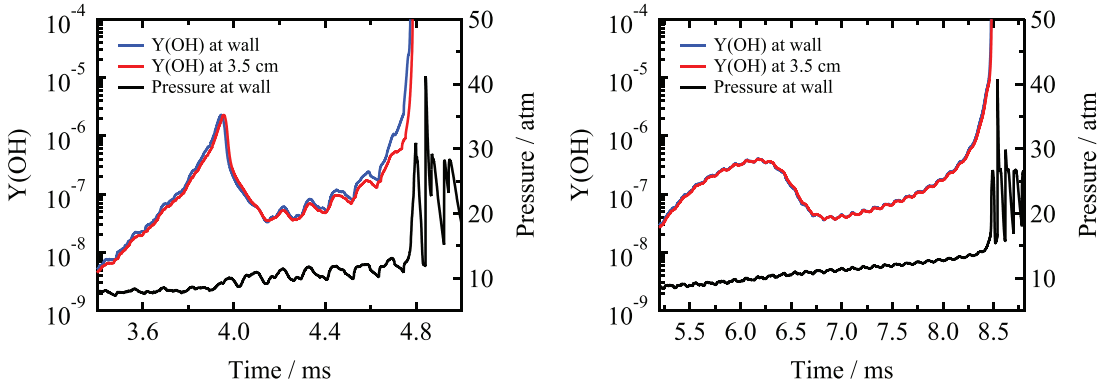

(a) DME (b) *n*-heptane

Fig. 9. Comparison of time histories of the mass fraction of OH between the wall and an end-gas point, and the pressure at the wall, for an initial temperature of 650 K.

To investigate the mechanism that produces large knocking intensities in the *n*-heptane and DME cases, a temporal sequence of pressure and temperature distributions at 650 K is provided in Fig. 6. For both cases, autoignition first takes place at the end wall ($x = 4.0$ cm). Then, the generated pressure wave is followed by a reaction front wave driven by successive autoignition phenomena. Consequently, a strong pressure wave is produced by the coupling between the pressure and reaction front waves. In the DME case, the maximum pressure reaches a considerable value of approximately 110 atm, while it is limited to a smaller value of approximately 55 atm in the *n*-heptane case. Such strong pressure waves are caused by the non-uniform occurrence of end-gas autoignition (the mechanism for the non-uniform end-gas autoignition is described in the next section, Section 4.2). As recognized with the temperature distributions in Fig. 6, the temperature in the local region near the wall increases faster compared to that in other end-gas regions. In the DME case, the local temperature rise near the wall is more pronounced than that in the *n*-heptane case, and thus a stronger pressure wave can develop during propagation in the end-gas region. The non-uniformity of end-gas autoignition is relatively weak in the *n*-heptane case, and the successive autoignition, which occurs ahead of the developing pressure wave, disturbs its further development (see the profile 7). For the *n*-butane and *i*-octane cases, the end-gas region is very small when end-gas autoignition takes place, as illustrated in Fig. 4(b). Therefore, there is not enough space for a pressure wave to develop.

4.2. A question on non-uniform autoignition and strong pressure wave

All the computations start with a uniform distribution in the end-gas region, and thus a uniform end-gas autoignition would be expected. Previous studies [18,19] addressed the mechanism for non-uniform autoignition in the end-gas region, in which it was demonstrated that the pulsed compression wave generated from the ignition kernel continuously propagated in the reactor and enhanced the progress of chemical reactions in the near-wall region through wave reflection at the wall. Consequently, non-uniform autoignition occurs in the end-gas region. Then, a question is raised: why is the non-uniformity of end-gas autoignition strengthened in the DME case and the NTC regime because the pulsed pressure wave and wall reflection occur in all the fuels and all the initial temperature conditions.

Figure 7 shows again the time histories of the pressure and temperature at the wall for each fuel, where the result of each fuel is replotted separately for better comparison. A comparison of the four fuels indicates that the difference between fuels with larger knocking intensities (*n*-heptane and DME) and those with smaller knocking intensities (*n*-butane and *i*-octane) lies in the presence of a small temperature rise caused by the heat release of LTO. Moreover, there is a significant difference in the temperature rise between *n*-heptane and DME: the temperature increase rate in the DME case is considerably larger than that in the *n*-heptane case, which likely causes the large pressure oscillations observed

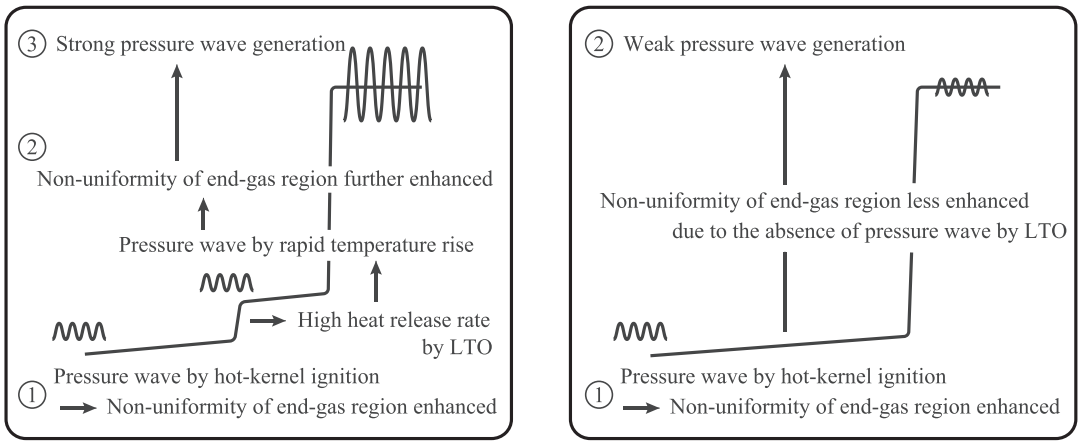

Fig. 10. Schematic of the role of low-temperature oxidation in strong pressure wave generation.

between approximately $t = 4$ and 5 ms in the DME case. Note that the pressure oscillation during the initial stage is caused by a pressure wave from the hot-kernel ignition, as described above.

Figure 8 (a) shows a temporal sequence of temperature distributions during LTO for the DME case. The temperature in the end-gas region rapidly changes between the profiles 4 and 5, which corresponds to the temperature rise at $t = 4$ ms in Fig. 7(a). This rapid and local change in the thermodynamic state in the end-gas region may induce large disturbance in the flow field, and thus a distinct (not sharp) pressure wave is generated, as illustrated in Fig. 8(b). In contrast, while the temperature rise by LTO also appears in the *n*-heptane case (Fig. 7(b)), the rate at which the temperature increase is relatively low, and thus a distinct pressure wave is barely generated. Therefore, it is concluded that the large pressure oscillation between LTO and the main autoignition is caused by the newly generated pressure wave due to the rapid temperature rise in LTO.

Once a pressure wave is generated in the reactor, it continuously propagates and reflects at the wall [18,19]. Thus, the reactivity in the end-gas region is affected, and, in particular, the wave reflection at the wall enhances the progress of chemical reactions through the transient pressure and temperature increases. When a temperature rise by LTO appears, pressure waves are generated by not only the hot-kernel ignition but also LTO. Figure 9(a) shows a comparison of the mass fraction of OH at an end-gas point ($x = 3.5$ cm) and the wall ($x = 4.0$ cm) in the DME case, where the pressure history at the wall is also plotted for comparison. The pressure oscillation after $t = 4.0$ ms corresponds to the transient pressure increase from the wall reflection, and thereby the mass fraction of OH transiently increases. The difference of the mass fraction of OH between two points gradually increases because the transient increase of pressure and temperature at the wall are more extensive than those at the end-gas point due to the wave reflection. Further, the result indicates that the induction period between the LTO and the main autoignition is vital for the enhancement of non-uniformity in the end-gas region because the difference in the mass fraction of OH at the two points in the end-gas region continues to increase during the induction period. In contrast, as shown in Fig. 9(b), the pressure oscillation is weak in the *n*-heptane case, and there is little difference in the mass fraction of OH between the two points.

In the cases of *n*-butane and *i*-octane, which generate no transient pressure and temperature rises in LTO, the non-uniformity of the end-gas region is solely caused by the pressure wave initially generated from the hot-kernel ignition. Therefore, the non-uniformity of end-gas autoignition is limited, and the pressure wave associated with end-gas autoignition does not develop. As

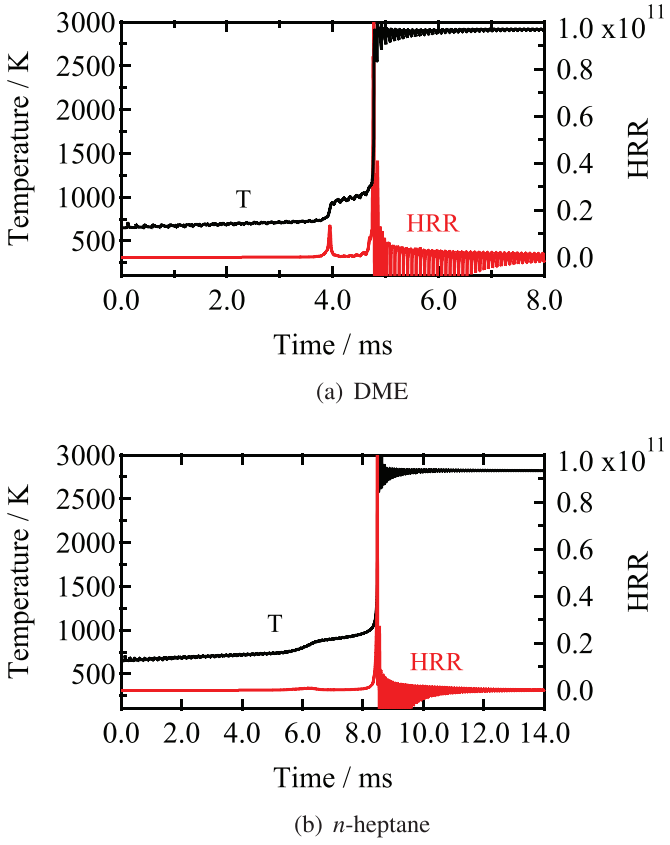

Fig. 11. Time histories of the temperature and heat release rate (HRR) at the wall for an initial temperature of 650 K. The unit of HRR is J m^{-3} s^{-1}.

such, in higher-temperature conditions, the temperature rise in LTO also disappears in the *n*-heptane and DME cases, as the result at 800 K is shown in Fig. 3(b). Thus, the non-uniformity of end-gas autoignition is not enhanced, and the knocking intensity tends to be small. Hence, the fuel dependency of the knocking intensity disappears in high-temperature conditions (see Fig. 5).

In summary, significant peak in the knocking intensity is generated in the DME case due to the non-uniformity in the end-gas region. The non-uniformity of end-gas autoignition is strengthened by the newly generated pressure wave, which is induced by the rapid temperature rise of the end-gas region during LTO. The continuous pressure wave reflection at the wall significantly enhances

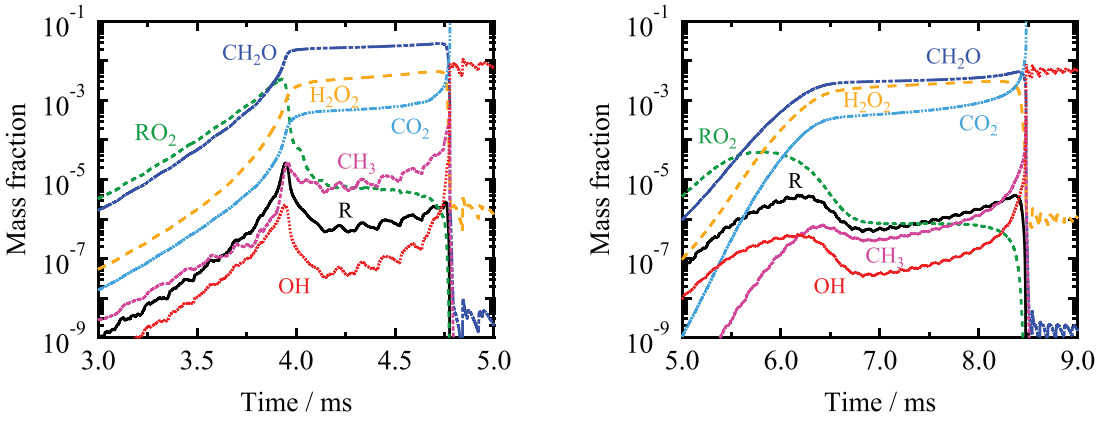

(a) DME, where R = CH_3OCH_2 (b) *n*-heptane, where R = *n*-C_7H_{15}

Fig. 12. Time histories of chemical species at the wall for an initial temperature of 650 K.

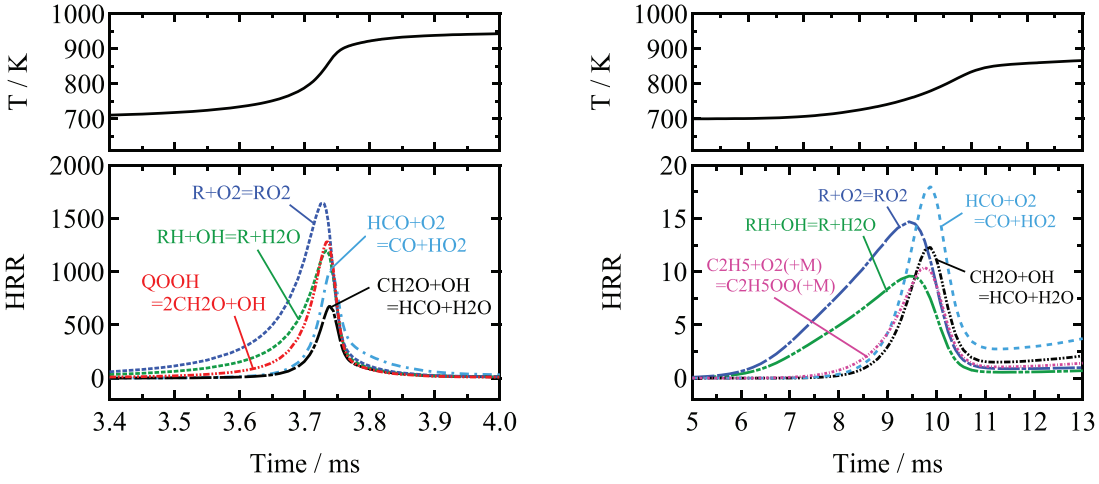

(a) DME, where R = CH_3OCH_2 and Q = CH_2OCH_2 (b) *n*-heptane, where R = *n*-C_7H_{15}

Fig. 13. Time histories of temperature and heat release rate of elementary reactions obtained in a 0-D constant-volume ignition problem, where top five elementary reactions with the highest heat release rate in LTO are presented. The initial temperature and pressure are 650 K and 5 atm, and a stoichiometric mixture is used for both cases. The unit of HRR is MJ m^{-3} s^{-1}.

the non-uniformity of end-gas autoignition. A schematic of the role of LTO in the strong pressure wave generation proposed in this study is illustrated in Fig. 10.

4.3. Heat release rate and chemical reactions in LTO

The rate of temperature increase in LTO is associated with the heat release rate of the chemical reactions. Figure 11 shows a comparison of the time histories of the heat release rate and temperature at the wall between the DME and *n*-heptane cases. It is confirmed that the rapid temperature rise in the DME case is associated with a higher heat release rate, and the heat release rate in the DME case is much higher than that in the *n*-heptane case during LTO.

To identify the source of the high heat release rate in the DME case, the time history of the mass fractions of several chemical species at the wall is presented in Fig. 12. A key difference between DME and *n*-heptane is in the production of CH_2O during LTO; a considerably larger amount of CH_2O is generated in the DME case compared to the *n*-heptane case. A large amount of CH_2O generally enhances the following chemical reactions responsible for the heat generation:

$$HO_2 + HO_2 \rightarrow H_2O_2 + O_2 \quad \Delta_r H_{298} = -164 \text{ kJ mol}^{-1} \tag{R1}$$

$$H_2O_2 + M \rightarrow OH + OH + M \quad \Delta_r H_{298} = 210 \text{ kJ mol}^{-1} \tag{R2}$$

$$CH_2O + OH \rightarrow HCO + H_2O \quad \Delta_r H_{298} = -128 \text{ kJ mol}^{-1} \tag{R3}$$

$$HCO + O_2 \rightarrow CO + HO_2 \quad \Delta_r H_{298} = -139 \text{ kJ mol}^{-1} \tag{R4}$$

which eventually lead to a high heat release rate and thus the rapid temperature rise of DME. The enthalpies of reaction, $\Delta_r H_{298}$, were taken from the *n*-heptane model [33].

The larger production of CH_2O in the DME case compared to that in the *n*-heptane case can be explained by the three following chemical reaction features. The first one is a larger production of RO_2 through a reaction of

$$R + O_2 \rightarrow RO_2 \tag{R5}$$

due to the higher ceiling temperature of DME, where R = CH_3OCH_2 (the ceiling temperature is defined as the temperature at which the equilibrium concentration of R equals that of RO_2). Secondly, the successive reactions after the RO_2 production reaction (R5) proceed through RO_2 → QOOH isomerization followed by the decomposition of QOOH to $2CH_2O + OH$. The production of CH_2O from DME

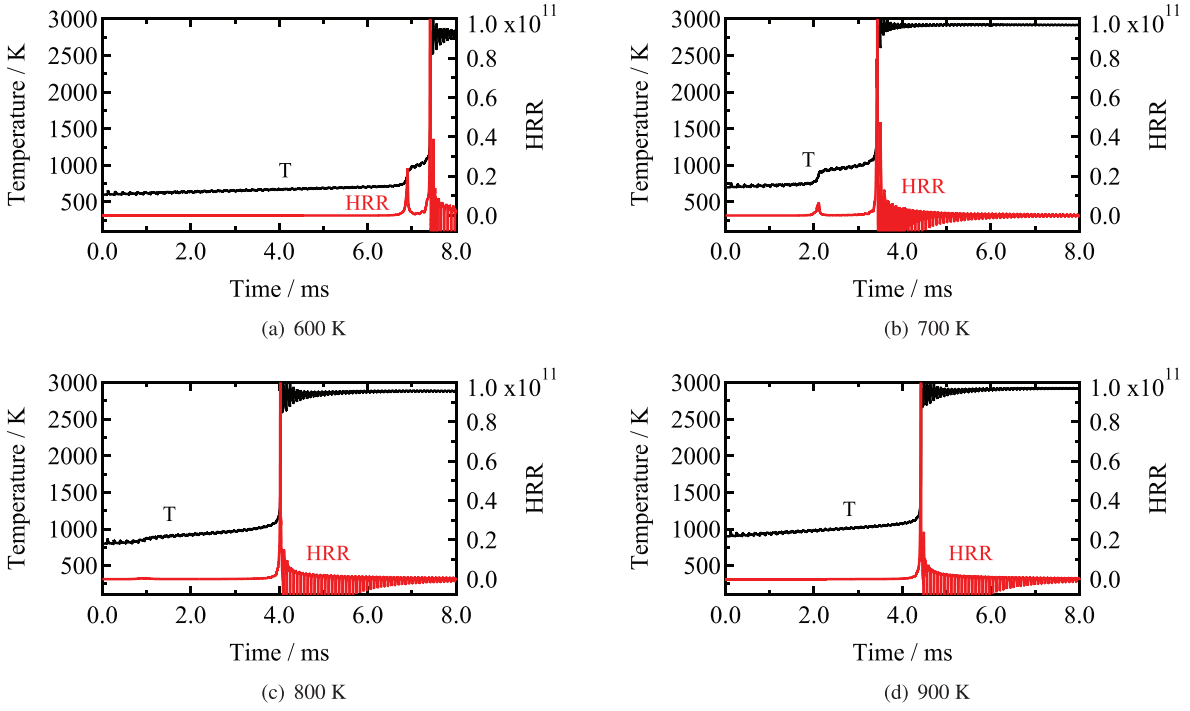

Fig. 14. Comparison of the evolution of temperature and heat release rate (HRR) for different initial temperatures in the DME case. The unit of HRR is J m^{-3} s^{-1}.

in this sequence is more efficient than that from the corresponding reactions of *n*-heptane due to the higher ceiling temperature of DME and the absence of cyclic ether formation in the DME case. The third one, which is considered to be the most important, is the production of CH_2O through the thermal decomposition,

$$CH_3OCH_2 \rightarrow CH_2O + CH_3 \quad \Delta_r H_{298} = 26 \text{ kJ mol}^{-1} \qquad \text{(R6)}$$

which is an endothermic reaction specific to DME and does not exist in the reaction of *n*-heptane. The enthalpy of reaction, $\Delta_r H_{298}$, were taken from the DME model [35]. Because the thermal decomposition (R6) is sensitive to the temperature, the heat generated through the reactions (R1) to (R4) accelerates the reaction (R6) and produces a further amount of CH_2O. This feedback loop brings about the high heat release rate in LTO. The larger production of CH_2O and CH_3 in the DME case can be confirmed in Fig. 12. Further, to confirm elementary reactions responsible for the heat release rate in LTO, the results of a zero-dimensional (0-D) constant-volume ignition problem obtained using ANSYS CHEMKIN-PRO are shown for the DME and *n*-heptane cases in Fig. 13. It is identified that, while similar elementary reactions are responsible for the heat release rate in LTO including (R3) and (R4) for both cases, the decomposition reaction of QOOH uniquely contributes to the heat release in the DME case, and DME produces much higher heat release rate compared to *n*-heptane in LTO.

Figure 14 shows the time histories of the temperature and heat release rate using four initial temperatures for DME. While the heat release rate in LTO is larger for lower initial temperatures, the induction period between the LTO and main autoignition is shortened. Thus, the non-uniformity is determined by a trade-off between the heat release rate and the induction period.

It may be worth noting the effect of initial pressure on the heat release rate in LTO. Figure 15 compares the first peak value of the heat release rate in LTO using a 0-D constant-volume ignition problem. The peak values increase in increasing the initial pressure for all three fuels: DME, *n*-heptane, and *i*-octane. Therefore, the strength of a pressure wave produced in LTO may be stronger under high-pressure conditions. The orders of peak values for *i*-octane at 20 atm and 40 atm become similar to those for *n*-heptane at 5 atm and DME at 5 atm, respectively, while the peak value for *i*-octane at 5 atm is very low.

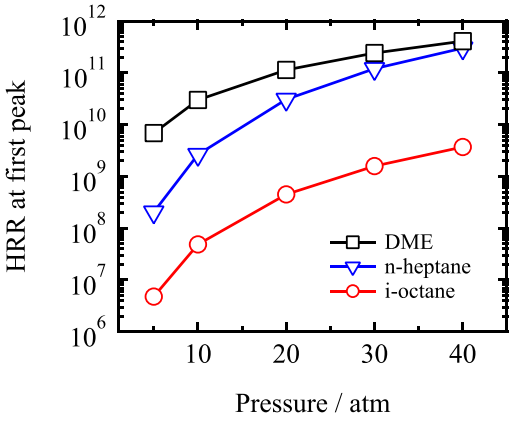

Fig. 15. Effects of pressure on the heat release rate in LTO for three fuels. The unit of HRR is J m^{-3} s^{-1}. The results were obtained using a 0-D constant-volume ignition problem. The initial temperature is 700 K and other initial temperature conditions show a similar trend.

4.4. Results with a smaller hot-kernel size

One may concern that another distinct pressure oscillation exists from the initial stage (for example, see Fig. 7), which is caused by a pressure wave generated from the hot-kernel ignition [18]. Thus, there are two individual events for pressure wave generation before end-gas autoignition: one is the pressure wave generated by the hot-kernel ignition, and the other is the pressure wave generated by the high heat release rate in LTO. While these pressure waves are weak compared to the strong pressure waves generated by end-gas autoignition, they play a significant role in establishing the non-uniformity of end-gas autoignition.

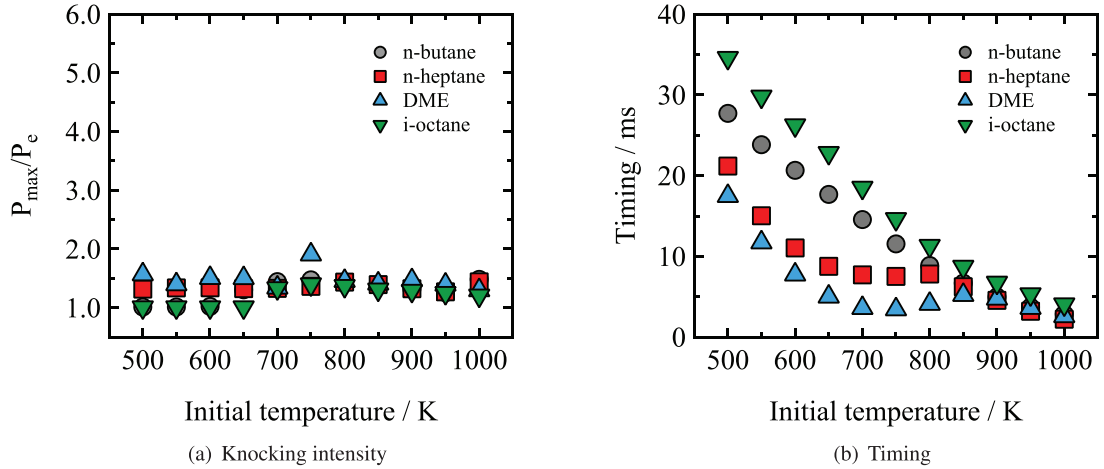

Fig. 16. Knocking intensity and timing for a small hot-kernel size of 0.05 cm.

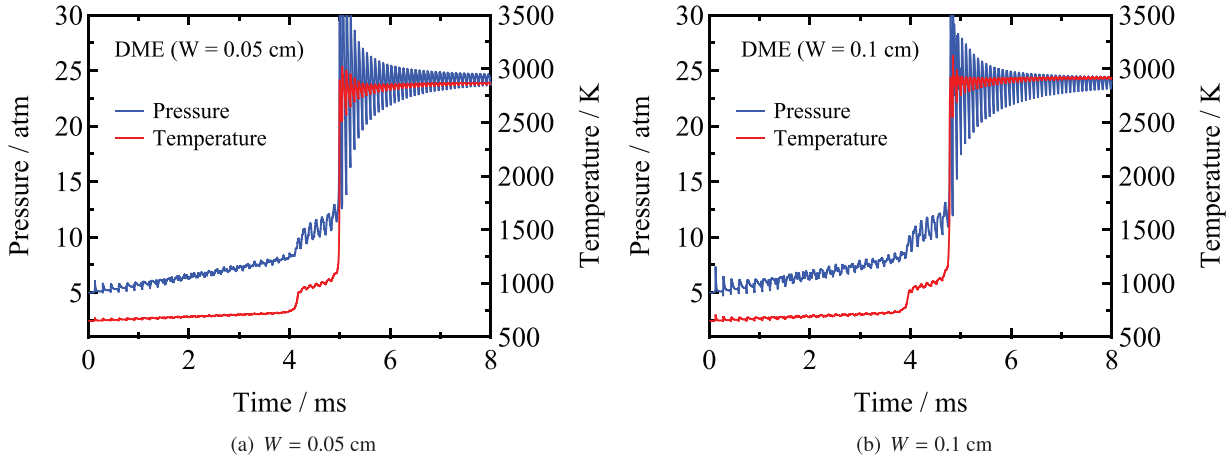

Fig. 17. Comparison of time histories of the pressure and temperature at the wall between two different kernels for the DME case. The results are for an initial temperature of 650 K.

To clarify the role of LTO, a computation using a different hot-kernel size was carried out, which weakened the strength of the pressure wave from the hot-kernel ignition, so that the pressure wave generated in LTO may be solely responsible for establishing the non-uniformity of end-gas autoignition.

Figure 16 shows the knocking intensity and timing obtained using the small hot-kernel size of 0.05 cm for all the fuel cases. There are no differences in the knocking timing from the result with the hot-kernel size of 0.1 cm shown in Fig. 4(a). In contrast, the large peaks in the knocking intensities for *n*-heptane and DME disappear with the smaller hot kernel. Therefore, the pressure wave from the ignition kernel also plays a significant role in establishing the non-uniformity of end-gas autoignition.

Figure 17 shows the time histories of the pressure and temperature at the wall for DME, with an initial temperature of 650 K, that were obtained using the smaller kernel; the result using the original kernel size of 0.1 cm is also plotted for comparison (the same as Fig. 7(a)). While the pressure oscillation caused by LTO is also observed with the smaller kernel size, the amplitude is slightly smaller than that with the larger kernel. It is also recognized that the amplitude of the pressure oscillation induced by the hot-kernel ignition during the initial stage becomes small. Figure 18 shows the time histories of the mass fraction of OH between the wall and an end-gas point, which were obtained using the smaller hot-kernel size. The difference between the two points is negligible compared to the result of the 0.1 cm ignition kernel in Fig. 9(a),

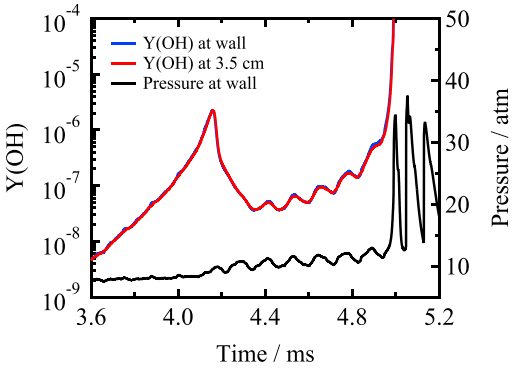

Fig. 18. Comparison of time histories of the mass fraction of OH between the wall and an end-gas point, and the pressure at the wall. The results are for an initial temperature of 650 K with a small hot-kernel size of 0.05 cm.

indicating that the non-uniformity in the end-gas region is less enhanced. Thus, these results suggest that the pressure wave generated in LTO alone may not be sufficient for establishing the non-uniformity of end-gas autoignition and producing strong pressure waves. The non-uniformity in the end-gas region needs to be established before LTO. In addition to the pressure wave from the ignition kernel addressed in the present study, other sources, such

as non-uniform concentration or temperature distributions, could establish the end-gas non-uniformity.

One may recognize in Fig. 16(a) that the small peak is generated at 750 K for DME. The small peak means that the pressure wave is developed because of a large end-gas region (see the flame position of DME in Fig. 4(b)). While a similar behavior is observed at different temperatures of 650 K and 700 K having large end-gas regions, the development of pressure waves is eventually disturbed by the occurrence of successive autoignition in front of the pressure wave. Unfortunately, a clear explanation for the different behaviors around 750 K has not been obtained at this point, while the result for $W = 0.05$ cm indicates that the length of the end-gas region affects the pressure wave development.

5. Conclusion

The role of LTO on end-gas autoignition and the subsequent pressure wave generation was numerically investigated. The results using four fuel/air stoichiometric mixtures were compared in the simulation using the compressible Navier–Stokes equations and a 1-D constant-volume reactor. Significant peaks of the knocking intensity were generated for the strong NTC fuels *n*-heptane and DME in their NTC regimes, where strong pressure waves developed owing to the non-uniform autoignition of the end-gas region. In particular, for the DME case, the non-uniformity in the end-gas region was significantly enhanced by distinct pressure wave disturbance generated by the high heat release rate in LTO. The non-uniformity was strengthened when the pressure wave was reflected at the wall during the induction period between the first ignition by LTO and the main autoignition. In contrast, these pressure wave disturbances were not generated in the weak NTC fuels *n*-butane and *i*-octane under the present conditions, and thus the knocking intensity was smaller due to the weaker non-uniformity of end-gas autoignition. The high heat release in LTO for the DME case was caused by the large production of CH_2O, mainly owing to the thermal decomposition reaction. This study concludes that the high heat release rate in LTO and the generated pressure wave disturbance play a significant role in the generation of large knocking intensities.

Declaration of Competing Interest

None.

Acknowledgments

This study was supported by JSPS KAKENHI Grant No. JP17K06939 and by the research association of automotive internal combustion engines (AICE). This study was also carried out under the collaborative research project No. J19I072 and No. J20I045 of the Institute of Fluid Science, Tohoku University. The first author appreciates the support from Mr. T. Nogawa and Mr. K. Keta of Hokkaido University.

References

[1] J.B. Heywood, Internal combustion engine fundamentals, McGraw-Hill, New York, 1988.
[2] Y.B. Zel'dovich, Regime classification of an exothermic reaction with nonuniform initial conditions, Combust. Flame 39 (1980) 211–214.
[3] X. Gu, D. Emerson, D. Bradley, Modes of reaction front propagation from hot spots, Combust. Flame 133 (2003) 63–74.
[4] Z. Wang, H. Liu, R.D. Reitz, Knocking combustion in spark-ignition engines, Prog. Energy Combust. Sci. 61 (2017) 78–112.
[5] M.J. Pilling, Low-temperature Combustion and Autoignition, Elsevier, 1997.
[6] P. Dai, Z. Chen, S. Chen, Y. Ju, Numerical experiments on reaction front propagation in n-heptane/air mixture with temperature gradient, Proc. Combust. Inst. 35 (2015) 3045–3052.
[7] P. Dai, Z. Chen, Supersonic reaction front propagation initiated by a hot spot in n-heptane/air mixture with multistage ignition, Combust. Flame 162 (2015) 4183–4193.
[8] P. Dai, C. Qi, Z. Chen, Effects of initial temperature on autoignition and detonation development in dimethyl ether/air mixtures with temperature gradient, Proc. Combust. Inst. 36 (2017) 3643–3650.
[9] C. Qi, P. Dai, H. Yu, Z. Chen, Different modes of reaction front propagation in n-heptane/air mixture with concentration non-uniformity, Proc. Combust. Inst. 36 (2017) 3633–3641.
[10] T. Zhang, W. Sun, Y. Ju, Multi-scale modeling of detonation formation with concentration and temperature gradients in n-heptane/air mixtures, Proc. Combust. Inst. 36 (2017) 1539–1547.
[11] T. Zhang, W. Sun, L. Wang, Y. Ju, Effects of low-temperature chemistry and turbulent transport on knocking formation for stratified dimethyl ether/air mixtures, Combust. Flame 200 (2019) 342–353.
[12] D. Bradley, Autoignitions and detonations in engines and ducts, Philos. Trans. R. Soc. Lond. Ser. A 370 (2012) 689–714.
[13] K. Tanoue, Y. Chado, T. Jimoto, T. Nomura, F. Shimada, J. Hashimoto, Effect of autoignition characteristics of fuels on knocking properties, Int. J. Engine Res. 17 (2016) 666–676.
[14] A. Mansfield, M. Wooldridge, H. Di, X. He, Low-temperature ignition behavior of iso-octane, Fuel 139 (2015) 79–86.
[15] J. Pan, Z. Hu, H. Wei, M. Pan, X. Liang, G. Shu, L. Zhou, Understanding strong knocking mechanism through high-strength optical rapid compression machines, Combust. Flame 202 (2019) 1–15.
[16] J. Pan, H. Wei, G. Shu, Z. Chen, P. Zhao, The role of low temperature chemistry in combustion mode development under elevated pressures, Combust. Flame 174 (2016) 179–193.
[17] H. Terashima, M. Koshi, Mechanisms of strong pressure wave generation in end-gas autoignition during knocking combustion, Combust. Flame 162 (2015) 1944–1956.
[18] H. Terashima, A. Matsugi, M. Koshi, Origin and reactivity of hot-spots in end–gas autoignition with effects of negative temperature coefficients: Relevance to pressure wave developments, Combust. Flame 184 (2017) 324–334.
[19] H. Terashima, A. Matsugi, M. Koshi, End-gas autoignition behaviors under pressure wave disturbance, Combust. Flame 203 (2019) 204–216.
[20] R. Kee, F. Ruply, J. Miller, CHEMKIN-II: a fortran chemical kinetics package for the analysis of gas-phase chemical kinetics, SAND89-8009 (1989).
[21] R. Kee, G. Dixon-Lewis, J. Warnatz, M. Coltrin, J. Miller, A fortran computer code package for the evaluation of gas-phase, multicomponent transport properties, SAND86-8246 (1986).
[22] J. Warnatz, U. Maas, R.W. Dibble, Combustion: Physical and Chemical Fundamentals, Modeling and Simulation, Experiments, Pollutant Formation, Springer, 2006.
[23] T. Lu, C.K. Law, Diffusion coefficient reduction through species bundling, Combust. Flame 148 (2007) 117–126.
[24] G. Strang, On the construction and comparison of difference schemes, SIAM J. Numer. Anal. 5 (1968) 506–517.
[25] R.P. Fedkiw, B. Merriman, S. Osher, High accuracy numerical methods for thermally perfect gas flows with chemistry, J. Comput. Phys. 132 (1997) 175–190.
[26] E.F. Toro, M. Spruce, W. Speares, Restoration of the contact surface in the HLL-Riemann solver, Shock Waves 4 (1994) 25–34.
[27] B.V. Leer, Flux-vector Splitting for the Euler equation, Springer, 1997.
[28] S. Gottlieb, C.W. Shu, Total variation diminishing Runge–Kutta schemes, Math. Comput. 67 (1998) 73–85.
[29] Y. Morii, H. Terashima, M. Koshi, T. Shimizu, E. Shima, ERENA: a fast and robust jacobian-free integration method for ordinary differential equations of chemical kinetics, J. Comput. Phys. 322 (2016) 547–558.
[30] Y. Ju, W. Sun, M.P. Burke, X. Gou, Z. Chen, Multi-timescale modeling of ignition and flame regimes of n-heptane-air mixtures near spark assisted homogeneous charge compression ignition conditions, Proc. Combust. Inst. 33 (2011) 1245–1251.
[31] H. Yu, Z. Chen, End-gas autoignition and detonation development in a closed chamber, Combust. Flame 162 (2015) 4102–4111.
[32] J. Pan, G. Shu, P. Zhao, H. Wei, Z. Chen, Interactions of flame propagation, auto-ignition and pressure wave during knocking combustion, Combust. Flame 164 (2016) 319–328.
[33] A. Miyoshi, KUCRS software library, See the web: http://akrmys.com/KUCRS/ for update information. The program uses THERM program for thermodata generation.
[34] A. Miyoshi, KUCRS-detailed kinetic mechanism generator for versatile fuel components and mixtures, Proceedings of the Eighth International Conference on Modeling and Diagnostics for Advanced Engine Systems (COMODIA 2012) (2012).
[35] Z. Zhao, M. Chaos, A. Kazakov, F.L. Dryer, Thermal decomposition reaction and a comprehensive kinetic model of dimethyl ether, Int. J. Chem. Kinet. 40 (2008) 1–18.